# Sensitivity to Hopf Bifurcation in Grid-Following Inverters Using Normal Vector Methods

Sushobhan Chatterjee <sup>®</sup> and Sijia Geng <sup>®</sup>

Abstract-With the increasing adoption of inverter-based resources (IBRs) in power systems, oscillations have become a significant challenge for system operators worldwide. This paper investigates the oscillatory instability of grid-following (GFL) inverters using Hopf bifurcation theory. We focus on examining how parameter variations affect the stability margin with respect to Hopf bifurcation. An analytical expression for the sensitivity of the stability margin is derived using the normal vector to the Hopf bifurcation hypersurface. Upon restructuring the differentialalgebraic equation (DAE) model of the GFL inverter into an ordinary differential equation (ODE) form, we identify the most effective control parameters for enhancing stability under varying operating conditions. It is shown that the normal vector method is efficient in estimating the stability margin in regard to both computational speed and accuracy. Results indicate that the proportional gain in the current control loop is the most effective parameter in improving the stability margin.

Index Terms—Hopf bifurcation, stability margin, gridfollowing inverter, oscillations, normal vectors, parameter sensitivity

# I. INTRODUCTION

Oscillations have received significant attention in the power system community since the late 20th century [1], mainly concerning the dynamics and stability of power systems dominated by conventional synchronous machines (SMs). However, with the increasing adoption of renewable energy and inverter-based resources (IBRs), it is becoming an alarming challenge for system operators to maintain system stability. For example, numerous sub-synchronous oscillation events that are attributed to IBRs have been observed worldwide [2], [3].

System and control parameters play a crucial role to prevent oscillatory instabilities in power systems. Most of the existing work in this domain investigates the issues from a linear systems perspective. Traditionally, this has been achieved by simplifying the model around a specific operating point and then adjusting the parameters of the linearized system to prevent instabilities. One of the key techniques the power systems engineers adopt is modal analysis which is based on eigenvalue and eigenvector computation [4]. Although useful in practice, only case-by-case results specific to the selected parameter and operating point can be obtained. An approach to address the challenge of numerous operating conditions is to develop robust stability criteria for a range of operating points, for example, in [5], [6]. Another idea is to characterize the stability boundary directly [7], [8]. Operating or designing a system to maintain stability across various

The authors are with the Department of Electrical and Computer Engineering, Johns Hopkins University. (email: schatt21@jhu.edu; sgeng@jhu.edu).

operating conditions can be seen as a geometric problem in a multidimensional parameter space [9]. It involves finding where the nominal parameters,  $\lambda_0$ , are located with respect to the hypersurfaces where stability is lost (i.e., bifurcations). Identifying the bifurcations closest to  $\lambda_0$  in the parameter space gives the stability margin. The parameter sensitivity of the stability margin guides the optimal parameter tuning to enhance stability robustness [10].

Table I summarizes a few works on bifurcations in power systems. [11] first proposed static bifurcation theory for voltage collapses arising in synchronous machine-driven systems. [12] posited a more complex nature of voltage crisis through the route of dynamic bifurcations. Later, the concept of chaos in power systems was analyzed in-depth using Lyapunov-Floquet theory by [13]–[16]. At the same time, the strategies for eliminating and controlling the undesirable nonlinear behaviors were proposed in [17]–[19]. Another line of work

TABLE I
KEY FEATURES OF THE PRIOR ART AND THIS WORK

References	Method	System	Bif'n	Control Scope	Parameter Sensitivity
[11]	Numerical	SM	Static	×	X
[12]	Numerical	SM	Static, Dynamic	×	X
[13]–[16]	Lyapunov- Floquet	SM	Static, Dynamic	×	×
[17]–[19]	Numerical	SM	Static, Dynamic	✓	×
[20]–[22]	Normal- Vector	SM	Static	✓	1
[23]	Numerical	IBR	Static, Dynamic	✓	×
[24], [25]	Numerical	SM-IBR	Static	×	×
This paper	Normal- Vector	IBR	Static	1	✓

involves analyzing parameter sensitivity towards bifurcations using the normal vector method [20]. Later, using the same idea, [21], [22] studied oscillatory instabilities in conventional power systems. The influence of parameters on the different bifurcations of grid-following (GFL) IBRs has been analyzed in [23] qualitatively. [24] studies the static voltage collapse in a mixed-sources system while [25] analyzes the static bifurcation phenomena in IBRs.

In this paper, we systematically analyze the parameter sensitivity to oscillation instability in GFL inverters with detailed modeling and control blocks. We tackle this problem using the normal vectors to Hopf bifurcation hypersurface and derive an analytical expression of the sensitivity of the stability margin

to parameter variation. We also investigate how the parameter sensitivities can be used to design efficient controls to restore system stability.

#### II. PRELIMINARIES

This section provides notational conventions used in the paper and preliminaries on power system modeling.

#### A. Notations

Let  $\mathbb{R}^n$  and  $\mathbb{C}^n$  be the space of n-dimensional real and complex vectors, respectively, and  $\mathbb{R}^{n \times n}$  be the space of real square matrices of order n. Let  $\mathbb{S}^n$  be a hypersphere of unit length in  $\mathbb{R}^n$ . Let  $I_n$  be the  $n \times n$  identity matrix. For a matrix  $A \in \mathbb{R}^{n \times n}$ ,  $\mu_i(A)$  denotes its ith eigenvalue. For a vector  $x \in \mathbb{C}^n$ ,  $x_i$  denotes its ith element,  $\bar{x}$  denotes its conjugate,  $x^T$  and  $x^H$  denotes its transpose and conjugate transpose (i.e.  $\bar{x}^T$ ), respectively, and  $\|x\|$  denotes its 2-norm unless stated otherwise. For a scalar x, |x| denotes its absolute value.  $\Re(x)$  denotes the real part of a complex number. For function f(x,y),  $D_x f$  denotes the partial derivative of f with respect to x.

## B. Reference Frames

Global reference frame: The widely used approach of creating a global rotating DQ-frame is adopted for converting sinusoidal quantities into approximately constant values. The rotational velocity (frequency) of this reference frame is given by  $\omega_{DQ}\omega_b$  rad/s, with  $\omega_{DQ}$  representing the per unit frequency of the DQ-frame and  $\omega_b$  the base frequency, e.g.,  $2\pi 50$  rad/s in Europe and most of Asia and  $2\pi 60$  rad/s in North America. Although it is common for  $\omega_{DQ}$  to be chosen as the nominal frequency  $\omega_0=1$ , it might have some related issues [26], [27]. For simplicity, we adopt the nominal value in our further analysis. Voltages and currents across the network are expressed in the global DQ-frame as,

$$v_t = v_{t,D} + jv_{t,Q},$$
  
 $i_t = i_{t,D} + ji_{t,Q}.$  (1)

Local reference: Each inverter uses a local dq-frame rotating at an angular frequency of  $(\omega + \omega_0)\omega_b$  rad/s, where the per unit frequency deviation  $\omega$  is determined by the inverter's internal mechanism, such as PLL or droop control. Voltages and currents at the inverter terminals are expressed in the local dq-frame as,

$$v_t = v_{t,d} + jv_{t,q},$$
  
 $i_t = i_{t,d} + ji_{t,q}.$  (2)

Reference frame transformation: To establish a uniform representation of the power system, it is necessary to convert the local dq-frame variables into the global DQ-frame. We define the rotation matrix  $\mathcal{R}(\theta)$ ,

$$\mathcal{R}(\theta) = \begin{bmatrix} \cos(\theta) & -\sin(\theta) \\ \sin(\theta) & \cos(\theta) \end{bmatrix}, \tag{3}$$

where the parameter  $\theta$  denotes the angle of the local dq-frame with respect to the global DQ-frame. The final transformation

can be expressed as,

$$\begin{bmatrix} v_{t,D} \\ v_{t,Q} \end{bmatrix} = \mathcal{R}(\theta) \begin{bmatrix} v_{t,d} \\ v_{t,q} \end{bmatrix},$$

$$\begin{bmatrix} i_{t,D} \\ i_{t,Q} \end{bmatrix} = \mathcal{R}(\theta) \begin{bmatrix} i_{t,d} \\ i_{t,q} \end{bmatrix}.$$
(4)

#### III. PROBLEM FORMULATION

Our primary objective is to analyze the stability boundary and parameter sensitivity associated with the oscillatory instability of IBRs. In this context, we first present the *normal vector* method and then derive an analytical expression for the parameter sensitivity of the stability margin to Hopf bifurcation.

# A. Bifurcation

Consider a system modeled by differential equations with parameters  $\lambda$ ,

$$\dot{x} = f(x, \lambda),\tag{5}$$

where  $f: \mathbb{R}^n \times \mathbb{R}^m \to \mathbb{R}^n$  is nonlinear and smooth,  $x \in \mathbb{R}^n$  are state variables and  $\lambda \in \mathbb{R}^m$  are the parameters. For parameter vector  $\lambda_0 \in \mathbb{R}^m$ , where  $\lambda_0$  represents the system's nominal or current parameters, we denote an equilibrium of (5) as  $x_0$  and assume it is asymptotically stable. As  $\lambda$  varies in the parameter space  $\mathbb{R}^m$ , the equilibrium  $x_0$  changes within the state space  $\mathbb{R}^n$  and might disappear or become unstable due to a bifurcation. If system (5) is assumed to have no special restrictions or structure, then saddle-node and Hopf bifurcations are the only bifurcations generic in curves of parameters, i.e., 1-d parameter variation in  $\mathbb{R}^m$  [28]. In this paper, we restrict to the study of Hopf bifurcations considering our focus on oscillation instability. This is due to the fact that, in general, sub-synchronous oscillations (SSO) arising in power systems are usually accompanied by strange nonlinear attractors born from the onset of Hopf bifurcations [29]. Hence, designing measures to prevent the system from approaching to the Hopf boundary becomes crucial for intercepting SSO. The formal definition of Hopf bifurcation is given below.

Definition 1: ([30], Hopf Bifurcation) Assume that f is a twice continuously differentiable function, and,

- 1)  $f(x_*, \lambda_*) = 0$ ,
- 2)  $f_x(x_*, \lambda_*)$  possess a simple pair of purely imaginary eigenvalues  $\mu(\lambda_*) = \pm j\omega_*$ ,  $\omega_* > 0$ , and does not have any other eigenvalues with zero real part,
- 3)  $D_{\lambda}(\Re{\{\mu(\lambda)\}})|_{*} \neq 0.$

Then, limit cycles bifurcate from the steady-state solution at the equilibrium point  $(x_*, \lambda_*)$ . This phenomenon is termed as Hopf bifurcation.

For the following analysis, we write  $x_*$  and  $\lambda_*$  for the equilibrium and parameters, respectively, at a (Hopf) bifurcation, and  $f_x|_* = f_x|_{(x_*,\lambda_*)}$  for the Jacobian  $f_x$  evaluated at the bifurcation. The hypersurfaces of the Hopf bifurcation, as denoted by  $\Sigma^H \subseteq \mathbb{R}^m$ , correspond to the set of  $\lambda_*$  for which equation (5) has a Hopf bifurcation at  $(x_*,\lambda_*)$ .

Given the parameter value  $\lambda_0$ , a key question is how close  $\lambda_0$  is to the set  $\Sigma^H$ . Since describing the shape of complex, multidimensional surfaces like  $\Sigma^H$  is very difficult, finding the points on  $\Sigma^H$  that are closest to  $\lambda_0$  is a practical way to

understand how  $\lambda_0$  relates to  $\Sigma^H$  without needing to describe the entire set. The directions from  $\lambda_0$  to these nearest points are the "worst case" scenarios for parameter changes that could make the system unstable. The distance from  $\lambda_0$  to the nearest points on  $\Sigma^H$  shows how stable the system is when operating at  $\lambda_0$ . If this distance is minimal, it indicates that the system is at risk, and the parameters should be adjusted to increase this distance. The optimal direction for making these adjustments can be determined by analyzing how sensitive the distance to the closest bifurcation is to parameter changes around  $\lambda_0$ .

# B. Normal Vectors to Hopf Bifurcation Hypersurfaces

Consider an eigenvalue  $j\omega_*$  of  $f_x|_{(x_*,\lambda_*)}$ . By definition, since  $f_x|_*$  is invertible, the implicit function theorem implies that there exists a smooth function u and a scalar constant  $\delta>0$ , defined in the neighbourhood of  $z_*:=(x_*,\lambda_*)$  such that,  $x=u(\lambda)$  and  $f(u(\lambda),\lambda)=0$ ,  $\forall \|z-z_*\| \leq \delta$ .

We can deduce an expression for  $u_{\lambda}$  as shown below. At an equilibrium,

$$\dot{x} = f(x, \lambda) = f(u(\lambda), \lambda) = 0. \tag{6}$$

We can write the total derivative,

$$D_{\lambda}\{f(u(\lambda),\lambda)\} = f_x(u(\lambda),\lambda)u_{\lambda}(\lambda) + f_{\lambda}(u(\lambda),\lambda) = 0,$$
(7)

and solve for,

$$u_{\lambda} = -f_x^{-1} f_{\lambda}. \tag{8}$$

Based on Kato's perturbation theorem [31, pp. 118], there exists a smooth function  $\mu$  defined in a neighbourhood of  $\lambda_*$ , such that  $\mu(\lambda) \in \mathbb{C}$  is an eigenvalue of  $f_x$ , with  $\mu(\lambda_*) = j\omega_*$ . As such, for eigenvalue  $\mu(\lambda)$  of  $f_x$ , we have  $f_xv = \mu(\lambda)v$  and  $w^Hf_x = w^H\mu(\lambda)$ , where  $v \in \mathbb{C}^n$  and  $w \in \mathbb{C}^n$  are the right and left eigenvectors, respectively. Normalizing v and w such that  $\|v\| = 1$  and  $w^Hv = 1$ , and pre-multiplying the right eigenvector equation by  $w^H$  yields an expression for  $\mu(\lambda)$ ,

$$w^H f_x v = \mu(\lambda) w^H v = \mu(\lambda). \tag{9}$$

We write  $v_*$  and  $w_*$  for the right and left complex eigenvector of  $f_x|_*$  corresponding to  $j\omega_*$ , and normalize them accordingly. Furthermore, using Wedin's theorem [32] to correlate perturbation of matrices with their invariant eigenspaces, it can be deduced from (9) that v and w are smooth functions of  $\lambda$  in a neighbourhood of  $\lambda_*$ . Thus, we can write  $v_* = v(\lambda_*)$  and  $w_* = w(\lambda_*)$ .

The non-degeneracy and transversality conditions that should be satisfied by  $\lambda_* \in \Sigma^H$  [33, pp. 352], are,

$$c_1|_* \neq 0,$$
  

$$D_{\lambda}(\Re\{\mu(\lambda)\})|_* \neq 0,$$
(10)

where  $c_1$  is a coefficient for the cubic terms in the flow reduced to the center manifold, which is proportional to the first Lyapunov coefficient and is a function of triple derivatives of f (c.f. [34, Sec 3.4] for more information). Non-degeneracy guarantees that  $\Sigma^H$  is locally a smooth hypersurface near  $\lambda_*$  and the transversality conditions ensure that the parameter variation crosses through the hypersurface transversally at  $\lambda_*$ . It follows that  $\Sigma^H$  has a normal vector  $\mathcal{N}(\lambda_*) \in \mathbb{R}^m$  at  $\lambda_* \in \Sigma^H$  and the Gauss map  $\mathcal{N}: \Sigma^H \to \mathbb{S}^m$  is smooth. Moreover, using the definition of transversality condition in (10), we can derive an expression for the normal vector to

Hopf bifurcation as,

$$\mathcal{N}(\lambda_*) := \beta D_{\lambda} \left( \Re\{\mu(\lambda)\} \right)_* 
= \beta D_{\lambda} \left( \Re\{w^H f_x v\} \right)_* 
= \beta \Re\left\{ \mu(\lambda) \left[ v^H w_{\lambda} + w^H v_{\lambda} \right] + w^H D_{\lambda} \left[ f_x(u(\lambda), \lambda) \right] v \right\}_* 
= \beta \Re\left\{ \mu(\lambda) D_{\lambda}(w^H v) + w^H \left[ f_{xx} u_{\lambda} + f_{x\lambda} \right] v \right\}_* 
= \beta \Re\left\{ w^H \left( - f_{xx} f_x^{-1} f_{\lambda} + f_{x\lambda} \right) v \right\}_*$$
(11)

where  $\beta \neq 0$  is a real scaling factor.  $|\beta|$  is chosen so that  $\|\mathcal{N}(\lambda_*)\| = 1$  and the sign of  $\beta$  is chosen so that changing  $\lambda$  in the direction of  $\mathcal{N}(\lambda_*)$  leads to the instability of the equilibrium. Define  $\mathbf{T} := (\mathbf{T}_1 \dots \mathbf{T}_n), \mathbf{T}_i \in \mathbb{R}^{n \times m}$ , as,

$$\mathbf{T} := -f_{xx}f_x^{-1}f_\lambda + f_{x\lambda}.$$

T is a rank-3 tensor of order  $n \times n \times m$ . Upon contraction with w using mode-2 and with v via mode-1 tensor product [35], it yields a vector in  $\mathbb{R}^m$ .

# C. Parameter Sensitivity of the Distance to Bifurcation

The distance to the closest bifurcation from a nominal parameter  $\lambda_0$ , denoted as  $\Delta(\lambda_0) = \|\lambda_* - \lambda_0\|$ , is termed the stability margin. If  $\Delta$  is small, adjusting  $\lambda_0$  to increase  $\Delta$  is beneficial. The optimal direction of first-order changes in  $\lambda_0$  to maximize  $\Delta$  is determined by the sensitivity  $\Delta_{\lambda_0} = \frac{\partial \Delta(\lambda_0)}{\partial \lambda_0}$ . That is, we regard the margin  $\Delta$  as a function of the parameters  $\lambda$  and aim to find the largest sensitivity  $\Delta_{\lambda_0} \in \mathbb{R}^m$  so that the margin may be improved by changing parameters in that direction.

Consider a parameter variation from  $\lambda_0$  along the direction  $k \in \mathbb{R}^m$ . The sensitivity  $\Delta_{\lambda_0}$  is a scaled projection of the normal vector along the direction of k, as depicted in Fig (1).

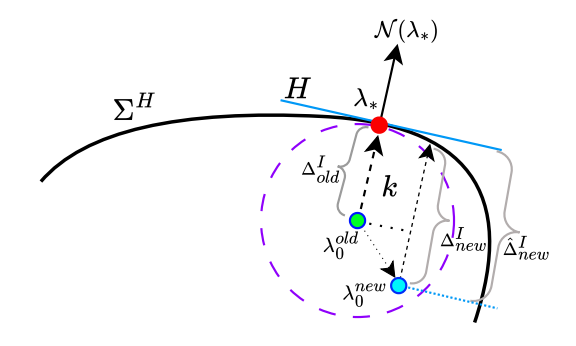


Fig. 1. Geometry of the bifurcation hypersurface, normal vectors, and the stability margin.

Utilizing the condition of encountering the first Hopf bifurcation as the parameters are varied in the direction k,

$$\Re\{\mu(\lambda_*)\} = 0,\tag{12}$$

we can write,

$$\frac{d}{d\lambda}\Re\{\mu(\lambda_*)\} = \frac{d}{d\lambda}\Re\{\mu(\lambda_0 + k\Delta(\lambda_0))\} = 0.$$
 (13)

This gives,

$$\mathcal{N}(\lambda_*)^T \left( I_m + k \Delta_{\lambda_0}^T \right) = 0, \tag{14}$$

which solves for an expression for the sensitivity as,

$$\Delta_{\lambda_0} = -\left[k^T \mathcal{N}(\lambda_*)\right]^{-1} \mathcal{N}(\lambda_*). \tag{15}$$

The parameters  $\lambda$  can often be divided into two types,  $\lambda = (\lambda^{uc}, \lambda^c)$ , where  $\lambda^{uc}$  represent uncontrollable parameters and  $\lambda^c$  are the controllable parameters. Typically, the variation of parameters  $\lambda^{uc}$  are not controllable by the operators or  $u_{dc}$  designers and may cause bifurcation, whereas  $\lambda^c$  contains design or control parameters that can be held constant or tuned. We aim to change the controllable parameters  $\lambda^c$  to ensure sufficient robustness concerning the variations of the uncontrollable parameters  $\lambda^{uc}$ . Towards this end, the normal vector may be partitioned as,

$$\mathcal{N} = (\mathcal{N}^{uc}, \mathcal{N}^c). \tag{16}$$

The parameter variation direction  $k = \{(k^{uc}, k^c) \mid k^c = 0\}$  has no components corresponding to  $\lambda^c$  so that  $k^T \mathcal{N}(\lambda_*) = (k^{uc})^T \mathcal{N}^{uc}(\lambda_*)$ . The sensitivity of the margin  $^1$  with respect to the controllable parameters  $\lambda^c$  is,

$$\Delta_{\lambda_0^c} = -\left[ (k^{uc})^T \mathcal{N}^{uc}(\lambda_*) \right]^{-1} \mathcal{N}^c(\lambda_*). \tag{17}$$

The sensitivities (17) can be used to identify the optimal controllable parameter in  $\lambda^c$  to adjust to increase the margin  $\Delta$ . More generally, optimization methods can be applied to maximize  $\Delta$ ; at the optimum, the sensitivity (17) becomes zero.

# IV. Model of Grid Following Inverters

Most inverter-based resources currently deployed on the grid are of the *grid-following* (GFL) type. These inverters are typically synchronized with the grid using phase-locked loops (PLLs) and inject a designated amount of active and reactive power. The analysis of this paper is carried out for a single-inverter-infinite-bus system as depicted in Fig. (2). We present a common GFL control for a PWM-based voltage source converter (VSC). Since our focus is on the system-level dynamics of IBRs, we make the following assumptions.

Assumption 1: The DC-side dynamics of the source are ignored. That is, the DC voltage  $u_{dc}$  remains fixed, while the DC current  $i_{dc}$  is an algebraic variable ensuring the required power supply to the inverter.

Assumption 2: The PWM switching dynamics are "fast enough" to be ignored, i.e., the inverter outputs voltage as the computed setpoints  $v_{t,d}$  and  $v_{t,q}$  instantaneously.

As shown in Fig. (2), the grid is represented as a rigid voltage source and the GFL inverter is connected to it through a transmission line as described in (42)-(43). The GFL inverter comprises a VSC with an output RLC filter described by (18)-(19) and (22)-(23). The controller has a hierarchical structure with an outer power-control loop and an inner current-control loop, as depicted in Fig. (3). The outer loop comprises the active (APC) (26) and reactive (RPC) (27) power controllers which are fed with power measurements (34)-(35). The reference signals produced by the outer control loops via (39)-(40), are sent to the inner current control (CC) loops as described by (20)-(21) and (30)-(31). The DC power balance equation is given in (41). The control loops are implemented in a local dqreference frame. A phase-locked loop (PLL) (24) generates the angle (25) and frequency (36) that are required to transform

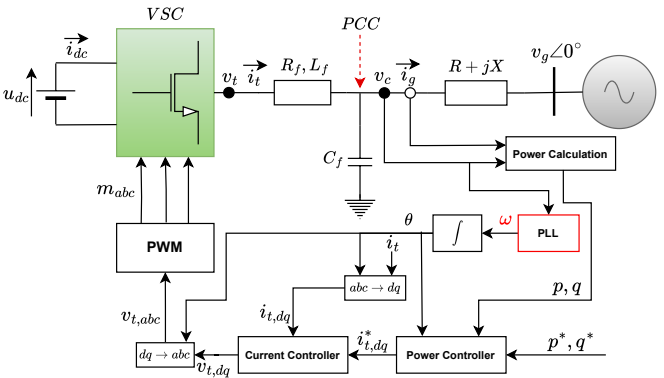


Fig. 2. GFL inverter connected to the grid.

three-phase voltage and current signals into dq quantities. The conversion of local quantities to the global DQ-frame is observed in (28)-(29), (32)-(33) and (37)-(38). The differential and algebraic equations for the system in Fig. (2) are given below and the nomenclature is provided in Appendix A.

# (1) Differential equations

$$\dot{i_{t,d}} = -\frac{R_f}{L_f} i_{t,d} + \omega i_{t,q} + \frac{1}{L_f} (v_{t,d} - v_{c,d})$$
(18)

$$\dot{i_{t,q}} = -\frac{R_f}{L_f} i_{t,q} - \omega i_{t,d} + \frac{1}{L_f} (v_{t,q} - v_{c,q})$$
(19)

$$\dot{\gamma}_d = i_{t,d}^* - i_{t,d} \tag{20}$$

$$\dot{\gamma}_q = i_{t,q}^* - i_{t,q}$$
 (21)

$$\dot{v}_{c,D} = \omega_g v_{c,Q} + \frac{1}{C_f} (i_{t,D} - i_{g,D})$$
 (22)

$$\dot{v}_{c,Q} = -\omega_g v_{c,D} + \frac{1}{C_f} (i_{t,Q} - i_{g,Q})$$
 (23)

$$\dot{\gamma}_{PLL} = v_{c,a} \tag{24}$$

$$\theta_{PLL}^{\cdot} = K_{PLL}^{P} v_{c,q} + K_{PLL}^{I} \gamma_{PLL} + \omega_s - \omega_g$$
 (25)

$$\dot{\phi}_d = p^* - p \tag{26}$$

$$\dot{\phi}_q = q^* - q \tag{27}$$

# (2) Algebraic equations

$$v_{c,d} - v_{c,D}\cos(\theta_{PLL}) - v_{c,O}\sin(\theta_{PLL}) = 0$$
 (28)

$$v_{c,q} + v_{c,D}\sin(\theta_{PLL}) - v_{c,Q}\cos(\theta_{PLL}) = 0$$
(29)

$$v_{t,d} - K_{CC}^{P}(i_{t,d}^{*} - i_{t,d}) - K_{CC}^{I}\gamma_{d} + \omega L_{f}i_{t,q} - K_{CC}^{F}v_{c,d} = 0$$
(30)

$$v_{t,q} - K_{CC}^{P}(i_{t,q}^{*} - i_{t,q}) - K_{CC}^{I} \gamma_{q} - \omega L_{f} i_{t,d} - K_{CC}^{F} v_{c,q} = 0$$
(31)

$$i_{t,D} - i_{t,d}\cos(\theta_{PLL}) + i_{t,q}\sin(\theta_{PLL}) = 0 \tag{32}$$

$$i_{t,Q} - i_{t,d}\sin(\theta_{PLL}) - i_{t,q}\cos(\theta_{PLL}) = 0$$
(33)

$$p - v_{c,d}i_{a,d} - v_{c,a}i_{a,g} = 0 (34)$$

$$q - v_{c,q}i_{g,d} + v_{c,d}i_{g,q} = 0 (35)$$

$$\omega - \omega_s - K_{PLL}^P v_{c,q} - K_{PLL}^I \gamma_{PLL} = 0 \tag{36}$$

$$i_{g,d} - i_{g,D}\cos(\theta_{PLL}) - i_{g,Q}\sin(\theta_{PLL}) = 0$$
(37)

$$i_{g,q} + i_{g,D} \sin(\theta_{PLL}) - i_{g,Q} \cos(\theta_{PLL}) = 0$$
 (38)

$$i_{t,d}^* - K_{APC}^P(p^* - p) - K_{APC}^I \phi_d = 0$$
(39)

<sup>&</sup>lt;sup>1</sup>Note that the margin here refers to the margin corresponding to the uncontrollable parameters.

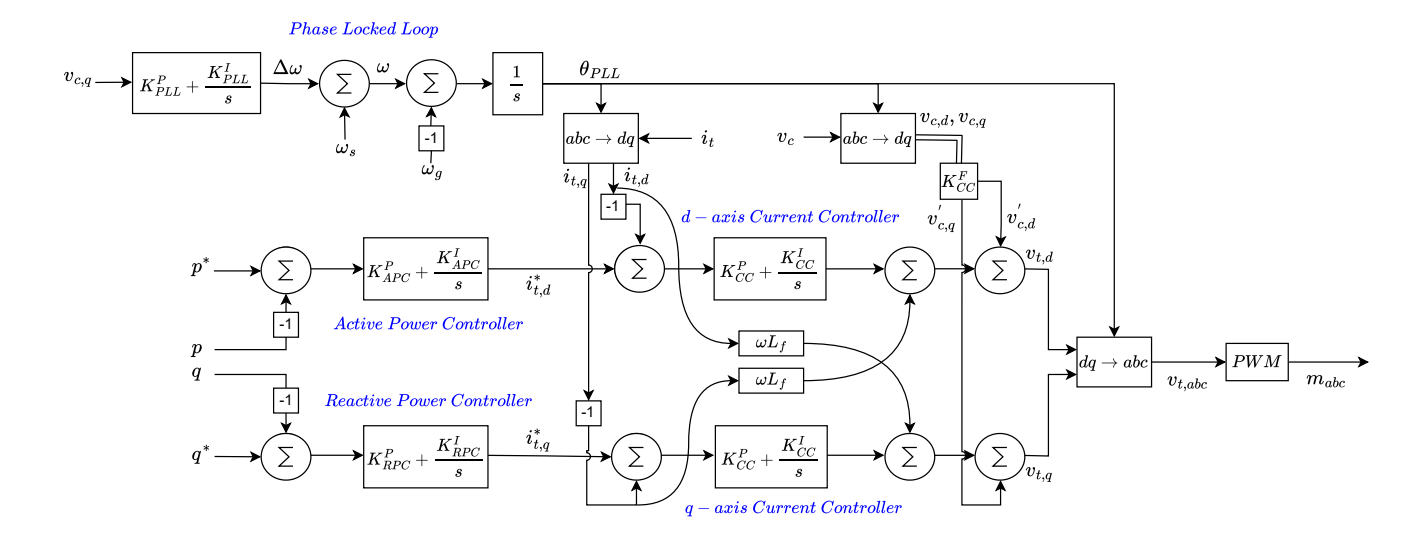


Fig. 3. Detailed control architecture of the GFL inverter.

$$i_{t,q}^* - K_{RPC}^P(q^* - q) - K_{RPC}^I \phi_q = 0$$
 (40)

$$u_{dc}i_{dc} - v_{t,d}i_{t,d} - v_{t,q}i_{t,q} = 0 (41)$$

$$i_{g,D} - \frac{R}{Z^2}(v_{c,D} - v_{g,D}) - \frac{X}{Z^2}(v_{c,Q} - v_{g,Q}) = 0$$
 (42)

$$i_{g,Q} - \frac{R}{Z^2}(v_{c,Q} - v_{g,Q}) + \frac{X}{Z^2}(v_{c,D} - v_{g,D}) = 0$$
 (43)

$$Z^2 - R^2 - X^2 = 0 (44)$$

Power system models are typically of the form of differential-algebraic equations (DAEs), such as the one given above for the single-inverter-infinite-bus system. One of the issues of the normal vector method is that it requires differential equations of index zero, that is, ODEs [36]. Hence, it is not directly applicable to positive *index* systems (i.e., DAEs) as is the case in our system. However, notice that the complex nonlinearity only appears in one state variable,  $\theta_{PLL}$ , while the rest are in bilinear form. We can explicitly solve the algebraic constraint equations to obtain the form y = f(x), and convert the set of DAEs into ODEs analytically. This leads to the restructured state equations in ODE form as given in the Appendix B. The transformation step eases the computation of the Jacobians and Hessians required for obtaining the normal vector, and a closed-form expression is obtained for the sensitivity in (17).

# V. NUMERICAL RESULTS

This section demonstrates the computation of parameter sensitivities to Hopf bifurcation using normal vectors and presents results for control tuning for GFL IBRs.

## A. System Setup

We consider base values of 20KVA and 400V for the system in Fig. 2. All the system variables and parameters are converted into per-unit quantities. In the IBR-based system, there are both controllable and uncontrollable parameters. Moreover, certain parameters may have larger impacts than the rest on the stability margin. In this work, we are interested in identifying

the most influential controllable parameters that will mitigate the impacts of the variation of uncontrollable parameters in order to design real-time actions to enhance system stability. The controllable and uncontrollable parameters of the *GFL* inverter-based system are identified as,

$$\begin{split} \lambda^{uc} &:= \left(R_f, L_f, C_f, \omega_g, \omega_s, v_{g,D}, v_{g,Q}, X, R\right) \in \mathbb{R}^9, \\ \lambda^c &:= \left(K_{PLL}^{P,I}, K_{CC}^{P,I,F}, K_{APC}^{P,I}, K_{RPC}^{P,I}, p^*, q^*\right) \in \mathbb{R}^{11}. \end{split}$$
 The nominal values of parameters are given in Table (II).

The nominal values of parameters are given in Table (II). When allowing a single parameter to vary, the parameter value when Hopf bifurcation occurs is provided in the table, where "-" denotes the parameters not analyzed for bifurcations (due to engineering consideration) and "X" denotes no bifurcation induced by the corresponding parameter.

 $\begin{tabular}{ll} TABLE II \\ SYSTEM AND CONTROL PARAMETERS FOR GFL \\ \end{tabular}$ 

Parameter	Nominal value (in p.u.)	Value at Hopf bifurcation (in p.u.)	Margin (in p.u.)
	· · · ·	birdication (in p.u.)	(III p.u.)
$R_f$	0.0072	-	-
$L_f$	0.2724	-	-
$C_f$	0.2612	-	-
$K_{PLL}^{P}$	2.65	0.0043	2.6457
$K_{PLL}^{I}$	6.5	1254.4	1247.9
$K_{CC}^{P}$	1.443	1.943	0.5
$K_{CC}^{IC}$	14.43	35.845	21.415
$K_{CC}^{I}$ $K_{CC}^{F}$	1	22.2125	21.2125
$K_{APC}^{P}$	1	2.0857	1.0857
$\frac{K_{APC}^{P}}{K_{APC}^{I}}$	3	98.267	95.267
$K_{RPC}^{P}$	-3	0.26032	2.7397
$K_{RPC}^{T}$	-4	-77.671	73.671
$\omega_g$	1	-	-
$p^{\overset{\omega}{*}}$	0.8	×	X
$q^*$	0.3	4.0707	3.7707
$\overline{X}$	0.07	0.07826	0.0083
R	0.02	0.01552	0.0045

From Table (II), it is clear that there is a large margin, i.e., the difference of the bifurcating value and the nominal value, in most of the integral gain parameters, especially  $K_{PLL}^{I}$ , towards inducing Hopf bifurcation. On the other hand, the

proportional gains exhibit the least robustness towards Hopf bifurcation. In the following sections, we will see how these observations are validated when the system is analyzed using normal vectors.

## B. Prediction of Stability Margin Using Normal Vectors

The undesirable bifurcation can be mitigated using the sensitivity information obtained through the normal vector method. We use a particular example to demonstrate the efficiency in estimating the stability margin using normal vectors. For example, consider an increase in the grid impedance X (i.e., weakening grid strength), and consider the parameter  $K_{CC}^P$  as the controllable parameter to alleviate the destabilizing effect of X. The sensitivity formula is given by (17), upon selecting the two parameters and the direction k (of increasing X). Using the sensitivity information, the predicted margin  $\hat{\Delta}_{new}^I$ , under the adjustment in the controllable parameter, is given by,

$$\hat{\Delta}_{new}^{I} = \Delta_{old}^{I} + \Delta_{\lambda_0}^{C|I} \left(\lambda_{new}^{C} - \lambda_{old}^{C}\right), \tag{45}$$
 where,  $I$  and  $C$  denote the indices of, the parameter causing

where, I and C denote the indices of, the parameter causing instability (X) and the control parameter  $(K_{CC}^P)$ , respectively. The true margin is obtained through numerical simulation, as,

$$\Delta_{new}^{I} = \Delta_{old}^{I} + (\lambda_{*,new}^{I} - \lambda_{*,old}^{I})$$

$$= (\lambda_{*,old}^{I} - \lambda_{0}^{I}) + (\lambda_{*,new}^{I} - \lambda_{*,old}^{I})$$

$$= \lambda_{*,new}^{I} - \lambda_{0}^{I}.$$
(46)

Note that the calculation of the predicted margin in (45) does not involve any simulations, contrary to that of the true margin in (46), which requires finding  $\lambda_{*,new}^{I}$  through simulation.

TABLE III
EFFECT OF PARAMETER VARIATION ON STABILITY MARGIN

$K_{CC}^{P}\downarrow$	Predicted Margin in X ↑	True Margin in X	Error
1.443 (Nominal)	-	0.00826	-
1.343	0.01028	0.010378	9.8e-05
1	0.017208	0.019439	2.23e-03
0.7	0.023268	0.030846	7.57e-03

Table (III) compares the true margin with the predicted margin using the normal vector method. The first row gives the nominal value of  $K_{CC}^P$  and the true nominal margin in X. The later rows show the reduction in  $K_{CC}^P$  and the corresponding increases in the margin in X, for the ground truth and the prediction, respectively. From Table (III), it is evident that the normal vector method is effective in predicting the sensitivity margins. Besides, the accuracy slightly decreases as the parameter values deviate from the nominal one. This is consistent with the fact that the prediction formula (45) is linear approximation whereas nonlinearities become more significant as conditions diverge from the nominal value.

## C. Control Parameter Sensitivity

We generate a normalized heatmap for the parameter sensitivities to Hopf bifurcation as depicted in Fig. (4). The parameters displayed on the y-axis of the map are responsible for causing Hopf bifurcation, whereas those on the x-axis represent the parameters to adjust to improve the margin. For example, based on the map, if the system encounters

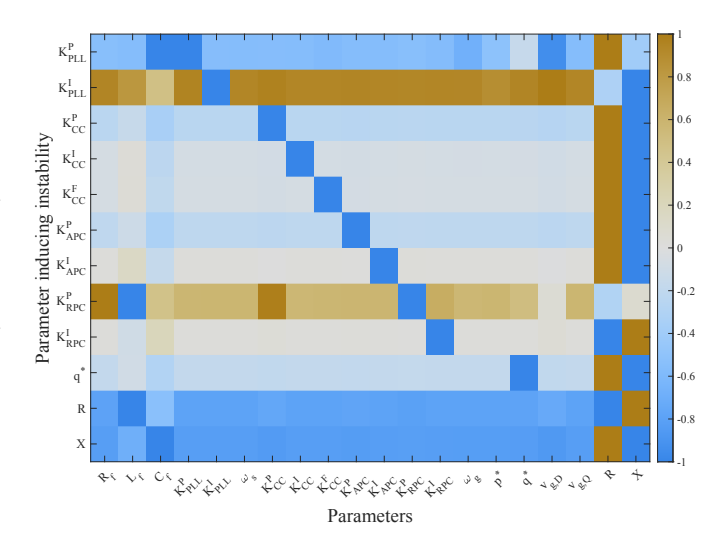


Fig. 4. Normalized heatmap of parameter sensitivities to Hopf bifurcation in GFL IBRs using min-max feature scaling.

instability due to increasing  $K^P_{RPC}$ , the most influential controllable parameter to go for would be increasing  $K^P_{CC}$ . It is worth mentioning that the entries with the same x and y indices hold no significance because it is always -1. In other words, if information is known on which parameter is inducing instability, the most effective remedy is always to alter that parameter in the opposite direction. Besides, the positive (negative) sensitivity values for control parameters may not necessarily indicate that increasing (decreasing) their values will increase the margin because it also depends on the direction in which the corresponding instability-inducing parameter is varied.

The most influential parameters that can be used in alleviating the instabilities induced by *other* parameters are summarized in Table (IV). The coloured up and down arrows indicate the direction in which the variation of parameters leads to instabilities. " $\mathbf{X}$ " implies an absence of Hopf bifurcation. The sensitivity  $\Delta_{\lambda_0}^{C|I}$  is given in per unit.

TABLE IV
MOST INFLUENTIAL CONTROL PARAMETERS FOR GFL

Cause of	Hopf Bifurcation		
instability (I)	Control (C)	Sensitivity $(\Delta_{\lambda_0}^{C I})$	
$K_{PLL}^{P} \downarrow$	$q^*$	0.03422	
$K_{PLL}^{TLL} \uparrow$	$p^*$	-746.706	
$K_{CC}^{P^{CL}} \uparrow$	$K_{APC}^{P}$	-0.63706	
$K_{CC}^{YC} \uparrow$	$K_{CC}^{P}$	-34.2752	
$K_{CC}^{FC} \uparrow \atop K_{APC}^{P} \uparrow$	$K_{CC}^{PC}$	-35.031	
$K_{APC}^{PC} \uparrow$	$K_{CC}^{PC}$	-2.9466	
$K_{APC}^{T} \uparrow$	$K_{CC}^{PC}$	-188.442	
$K_{RPC}^{P} \uparrow K_{RPC}^{I} \downarrow$	$K_{CC}^{PC}$	0.388007	
$K_{PPC}^{IIC} \downarrow$	$K_{CC}^{PC}$	162.034	
$p^*$	×	×	
$q^* \uparrow$	$K_{CC}^{P}$	-11.7163	
$X \uparrow$	$K_{CC}^{PC}$	-0.0202	
$R \downarrow$	$K_{CC}^{PC}$	0.009611	

It can be observed from Table (IV) that for Hopf bi-

furcations,  $K_{CC}^{P}$  turns out to be the most effective control parameter for steering away from oscillatory instability that is induced by variation of most of the parameters. The only exceptions are the parameter variations of the PLL control loop, for which the most effective control action is to tune the power setpoints. This consistency in the effectiveness of  $K_{CC}^{P}$  makes sense intuitively because the current controller in GFL is the last line of action towards establishing a gridfollowing nature. This observation is useful in the sense that, no matter which parameter's variation is causing the reduction in stability margin or even bifurcation, the most effective control action is to tune the  $K_{CC}^{P}$  (under the considered operating point). Another interesting observation is that the active power setpoint  $p^*$  is not inducing Hopf bifurcation in the standard GFL model considered in this work.

# VI. CONCLUSION

This paper studied the impacts of parameter variations on the stability margin of grid-following inverters to Hopf bifurcation. Normal vectors to the Hopf bifurcation hypersurface were employed to derive an analytical expression for the sensitivity of the stability margin, which is then used to conduct a systematic investigation spanning the entire parameter space of the GFL inverter-based system. The analysis identified a consistent control parameter, that is, the proportional gain of the current control loop, in steering the system away from Hopf bifurcation, regardless of which parameter is inducing instability. Note that, upon the construction of the normal vector, the complete information on the parameter sensitivity can be obtained, which is much more computationally efficient than conducting numerical simulations to find the stability margin for all the parameter variations. Ongoing and future work aims to improve the scalability of the method to larger networks and extend the method to hybrid dynamical systems with switching algebraic equations.

## **APPENDIX**

#### A. Nomenclature

The indexing of the variables and parameters used in the

```
differential and algebraic equations is described below.
Dynamic states (10):
x_1: i_{t,d} \to (\text{Local}) \text{ d-axis IBR output current } i_t
x_2: i_{t,q} \to (\text{Local}) \text{ q-axis IBR output current } i_t
x_3: \gamma_d \to \text{d-axis} current controller state
x_4: \gamma_q \to \text{q-axis current controller state}
x_5: v_{c,D} \to \text{(Global) D-axis filter output voltage } v_c
x_6: v_{c,Q} \to \text{(Global) Q-axis filter output voltage } v_c
x_7: \gamma_{PLL} \to \text{PLL} integrator state
x_8: \theta_{PLL} \to \text{PLL} phase angle
x_9: \phi_d \to \text{d-axis} (active) power controller state
x_{10}: \phi_q \rightarrow \text{q-axis} (reactive) power controller state
Algebraic states (17):
y_1: v_{t,d} \to \text{d-axis IBR output voltage } v_t
y_2: v_{t,q} \to \text{q-axis IBR output voltage } v_t
y_3:\omega\to {
m IBR} angular frequency determined by PLL
```

 $y_4: i_{t,d}^* \to \text{d-axis current setpoint } i_t^*$ 

 $v_{c,O}\cos(\theta_{PLL})$  $\dot{\gamma}_d = K_{APC}^P \ p^* - K_{APC}^P \left( \frac{R}{Z^2} \left[ v_{c,D}^2 + v_{c,Q}^2 - v_{c,D} v_{g,D} \right] \right)$ 

 $\frac{R}{Z^2}v_{c,Q}v_{g,D} - \frac{K_{CC}^F - 1}{L_f} \left[ v_{c,D}\sin(\theta_{PLL}) - \right]$ 

 $i_{t,d} = -\frac{1}{L_{t}} (R_f + K_{CC}^P) i_{t,d} + \frac{K_{CC}^I}{L_{t}} \gamma_d + \frac{K_{CC}^P K_{APC}^I}{L_{t}} \phi_d$ 

 $\frac{X}{Z^2}v_{c,Q}v_{g,D} + \frac{K_{CC}^F - 1}{L_f} \left[ v_{c,D}\cos(\theta_{PLL}) + \right]$ 

 $i_{t,q} = -\frac{1}{L_f} (R_f + K_{CC}^P) i_{t,q} + \frac{K_{CC}^I}{L_f} \gamma_q + \frac{K_{CC}^P K_{RPC}^I}{L_f} \phi_q$ 

 $+ \, \frac{K_{CC}^P K_{RPC}^P}{L_F} \bigg( q^* - \frac{X}{Z^2} \big[ v_{c,D}^2 + v_{c,Q}^2 - v_{c,D} v_{g,D} \big] \, + \\$ 

 $+\frac{K_{CC}^{P}K_{APC}^{P}}{L_{f}}\left(p^{*}-\frac{R}{Z^{2}}\left[v_{c,D}^{2}+v_{c,Q}^{2}-v_{c,D}v_{g,D}\right]\right)$ 

Parameters (19):  $p_1: R_f \to \text{Filter resistance}$  $p_2: L_f \to \text{Filter inductance}$  $p_3: C_f \to \text{Filter capacitance}$  $p_4: K_{PLL}^P \to \text{Proportional gain of PLL}$  $p_5: K_{PLL}^I \to \text{Integral gain of PLL}$  $p_6: \omega_s \to \text{Synchronous angular frequency for IBR}$  $p_7: K_{CC}^P \to \text{Proportional gain of current controller}$  $p_8: K_{CC}^I \to \text{Integral gain of current controller}$  $p_9: K_{CC}^F \to \text{Feed-forward gain of current controller}$  $p_{10}: K_{APC}^P \to \text{Proportional gain of active power controller}$  $p_{11}: K_{APC}^I \to \text{Integral gain of active power controller}$  $p_{12}: K_{RPC}^P \to \text{Proportional gain of reactive power controller}$  $p_{13}: K_{RPC}^I \to \text{Integral gain of reactive power controller}$  $p_{14}: \omega_g \to \text{Grid angular frequency}$  $p_{15}: p^* \to \text{Active power setpoint}$  $p_{16}: q^* \to \text{Reactive power setpoint}$  $p_{17}: v_{q,D} \to \text{D-axis Grid voltage } v_q$  $p_{18}: v_{g,Q} \to Q$ -axis Grid voltage  $v_g$  $p_{19}: R \to \text{Transmission line resistance}$  $p_{20}: X \to \text{Transmission line reactance}$ B. Restructured System Equations We analytically eliminate the algebraic variables from the DAEs in Sec. (IV) to obtain the following ODEs for the GFL-

 $y_5: i_{t,q}^* \to \text{q-axis current setpoint } i_t^*$ 

 $y_6: i_{t,D} \to \text{D-axis IBR output current } i_t$ 

 $y_7: i_{t,Q} \to \text{Q-axis IBR output current } i_t$ 

 $y_8: v_{c,d} \to \text{d-axis}$  filter output voltage  $v_c$ 

 $y_9 : v_{c,q} o ext{q-axis}$  filter output voltage  $v_c$  $y_{10}: p \rightarrow \text{Active power output from filter}$ 

 $y_{11}: q \to \text{Reactive power output from filter}$ 

 $y_{12}:i_{g,d}\to \text{d-axis}$  filter output current  $i_g$ 

 $y_{13} \; : \; i_{g,q} 
ightarrow ext{q-axis filter output current } i_g$ 

 $y_{14}:i_{g,D}\to ext{D-axis}$  filter output current  $i_g$ 

 $y_{15}:i_{g,Q}\to ext{Q-axis}$  filter output current  $i_g$ 

 $y_{16}: u_{dc} \rightarrow \text{DC-link voltage}$ 

 $y_{17}:i_{dc}\to \text{DC-link current}$ 

based system.

 $v_{c,Q}\sin(\theta_{PLL})$ 

$$\begin{split} & + \frac{X}{Z^{2}}v_{c,Q}v_{g,D} \Big) + K_{APC}^{I} \ \phi_{d} - i_{t,d} \\ & \dot{\gamma_{q}} = K_{RPC}^{P} \ q^{*} - K_{RPC}^{P} \Big( \frac{X}{Z^{2}} \big[ v_{c,D}^{2} + v_{c,Q}^{2} - v_{c,D}v_{g,D} \big] \\ & - \frac{R}{Z^{2}}v_{c,Q}v_{g,D} \Big) + K_{RPC}^{I} \ \phi_{q} - i_{t,q} \\ & v_{c,D} = \omega_{g}v_{c,Q} + \frac{1}{C_{f}} \Big( i_{t,d}\cos(\theta_{PLL}) - i_{t,q}\sin(\theta_{PLL}) - \frac{R}{Z^{2}} \big[ v_{c,D} - v_{g,D} \big] - \frac{X}{Z^{2}}v_{c,Q} \Big) \\ & v_{c,Q} = -\omega_{g}v_{c,D} + \frac{1}{C_{f}} \Big( i_{t,d}\sin(\theta_{PLL}) + i_{t,q}\cos(\theta_{PLL}) + \frac{X}{Z^{2}} \big[ v_{c,D} - v_{g,D} \big] - \frac{R}{Z^{2}}v_{c,Q} \Big) \\ & \gamma_{PLL} = -v_{c,D}\sin(\theta_{PLL}) + v_{c,Q}\cos(\theta_{PLL}) \\ & \theta_{PLL} = K_{PLL}^{P} \Big( -v_{c,D}\sin(\theta_{PLL}) + v_{c,Q}\cos(\theta_{PLL}) + K_{PLL}^{I}\gamma_{PLL} + \omega_{s} - \omega_{g} \\ & \dot{\phi}_{d} = p^{*} - \Big( \frac{R}{Z^{2}} \big[ v_{c,D}^{2} + v_{c,Q}^{2} - v_{c,D}v_{g,D} \big] - \frac{R}{Z^{2}}v_{c,Q}v_{g,D} \Big) \\ & \dot{\phi}_{q} = q^{*} - \Big( \frac{X}{Z^{2}} \big[ v_{c,D}^{2} + v_{c,Q}^{2} - v_{c,D}v_{g,D} \big] - \frac{R}{Z^{2}}v_{c,Q}v_{g,D} \Big) \end{split}$$

#### REFERENCES

- O. W. Hanson, C. Goodwin, and P. L. Dandeno, "Influence of excitation and speed control parameters in stabilizing intersystem oscillations," *IEEE Transactions on Power Apparatus and Systems*, no. 5, pp. 1306– 1313, 1968.
- [2] Y. Cheng, L. Fan, J. Rose, S.-H. Huang, J. Schmall, X. Wang, X. Xie, J. Shair, J. R. Ramamurthy, N. Modi, et al., "Real-world subsynchronous oscillation events in power grids with high penetrations of inverter-based resources," *IEEE Transactions on Power Systems*, vol. 38, no. 1, pp. 316– 330, 2022.
- [3] N. Modi, E. M. Farahani, A. Jalali, J. Ramamurthy, C. Chin, and B. Soetantijo, "Replication of real-world sub-synchronous oscillations in inverter-based resources dominated grid," *IEEE Transactions on Power Delivery*, 2024.
- [4] S. Okubo, H. Suzuki, and K. Uemura, "Modal analysis for power system dynamic stability," *IEEE Transactions on Power Apparatus and Systems*, no. 4, pp. 1313–1318, 1978.
- [5] R. Pates and E. Mallada, "Robust scale-free synthesis for frequency control in power systems," *IEEE Transactions on Control of Network* Systems, vol. 6, no. 3, pp. 1174–1184, 2019.
- [6] Z. Siahaan, E. Mallada, and S. Geng, "Decentralized stability criteria for grid-forming control in inverter-based power systems," in 2024 IEEE Power & Energy Society General Meeting (PESGM). IEEE, 2024.
- [7] B. De Dier, D. Roose, and P. Van Rompay, "Interaction between fold and Hopf curves leads to new bifurcation phenomena," *Continuation Techniques and Bifurcation problems*, pp. 171–186, 1990.
- [8] D. Wu, F.-E. Wolter, and S. Geng, "Approximating voltage stability boundary under high variability of renewables using differential geometry," *Electric Power Systems Research*, vol. 236, p. 110716, 2024.
- [9] I. Dobson, "Observations on the geometry of saddle node bifurcation and voltage collapse in electrical power systems," *IEEE Transactions on Circuits and Systems I: Fundamental Theory and Applications*, vol. 39, no. 3, pp. 240–243, 1992.
- [10] I. Dobson, "Distance to bifurcation in multidimensional parameter space: Margin sensitivity and closest bifurcations," *Bifurcation control: theory and applications*, pp. 49–66, 2003.
- [11] I. Dobson, H.-D. Chiang, J. S. Thorp, and L. Fekih-Ahmed, "A model of voltage collapse in electric power systems," in *Proceedings of the* 27th IEEE Conference on Decision and Control, pp. 2104–2109, IEEE, 1009
- [12] H. Wang, E. H. Abed, and A. M. Hamdan, "Is voltage collapse triggered by the boundary crisis of a strange attractor?," in 1992 American Control Conference, pp. 2084–2088, IEEE, 1992.
- [13] C. W. Tan, M. Varghese, P. Varaiya, and F. Wu, "Bifurcation and chaos in power systems," *Sadhana*, vol. 18, pp. 761–786, 1993.

- [14] H.-D. Chiang, C.-W. Liu, P. P. Varaiya, F. F. Wu, and M. G. Lauby, "Chaos in a simple power system," *IEEE Transactions on Power Systems*, vol. 8, no. 4, pp. 1407–1417, 1993.
- [15] J. Hongjie, Y. Yixin, Y. Xiaodan, H. Chunhua, and Z. Pei, "Three routes to chaos in power systems," in *Canadian Conference on Electrical* and Computer Engineering 2004 (IEEE Cat. No. 04CH37513), vol. 1, pp. 79–84, IEEE, 2004.
- [16] D. Wu, P. Vorobev, S. C. Chevalier, and K. Turitsyn, "Modulated oscillations of synchronous machine nonlinear dynamics with saturation," *IEEE Transactions on Power Systems*, vol. 35, no. 4, pp. 2915–2925, 2019.
- [17] H. O. Wang and E. H. Abed, "Control of nonlinear phenomena at the inception of voltage collapse," in 1993 American control conference, pp. 2071–2075, IEEE, 1993.
- [18] H. O. Wang, E. H. Abed, and A. M. Hamdan, "Voltage collapse dynamics and control in a sample power system," *IFAC Proceedings Volumes*, vol. 26, no. 2, pp. 825–828, 1993.
- [19] K. Srivastava and S. Srivastava, "Elimination of dynamic bifurcation and chaos in power systems using FACTS devices," *IEEE Transactions on Circuits and Systems I: Fundamental Theory and Applications*, vol. 45, no. 1, pp. 72–78, 1998.
- [20] I. Dobson, "An iterative method to compute a closest saddle node or Hopf bifurcation instability in multidimensional parameter space," in Proc. of the IEEE International Symposium on Circuits & Systems, San Diego, CA, pp. 2513–2516, 1992.
- [21] I. Dobson, F. Alvarado, and C. L. DeMarco, "Sensitivity of Hopf bifurcations to power system parameters," in [1992] Proceedings of the 31st IEEE Conference on Decision and Control, pp. 2928–2933, IEEE, 1992
- [22] I. Dobson and L. Lu, "New methods for computing a closest saddle node bifurcation and worst case load power margin for voltage collapse," *IEEE Transactions on Power Systems*, vol. 8, no. 3, pp. 905–913, 1993.
- [23] J. Yang, K. T. Chi, M. Huang, and D. Liu, "Bifurcations of grid-following rectifiers and routes to voltage instability in weak AC grids," *IEEE Transactions on Power Systems*, vol. 38, no. 2, pp. 1702–1713, 2022.
- [24] J. Choi, M. S. Illindala, A. Mondal, A. A. Renjit, and M. C. Pulcherio, "Cascading collapse of a large-scale mixed source microgrid caused by fast-acting inverter-based distributed energy resources," *IEEE Transactions on Industry Applications*, vol. 54, no. 6, pp. 5727–5735, 2018.
- [25] N. Hosseinzadeh, A. Aziz, A. Mahmud, A. Gargoom, and M. Rabbani, "Voltage stability of power systems with renewable-energy inverterbased generators: A review," *Electronics*, vol. 10, no. 2, p. 115, 2021.
- [26] D. Venkatramanan, M. K. Singh, O. Ajala, A. Dominguez-Garcia, and S. Dhople, "Integrated system models for networks with generators & inverters," in *Proceedings of the 11th Bulk Power Systems Dynamics* and Control Symposium (IREP), 2022.
- [27] S. Geng and I. A. Hiskens, "Unified grid-forming/following inverter control," *IEEE Open Access Journal of Power and Energy*, vol. 9, pp. 489–500, 2022.
- [28] J. Sotomayor, "Generic bifurcations of dynamical systems," in *Dynamical systems*, pp. 561–582, Elsevier, 1973.
- [29] M. Varghese, F. Wu, and P. Varaiya, "Bifurcations associated with subsynchronous resonance," *IEEE transactions on power systems*, vol. 13, no. 1, pp. 139–144, 1998.
- [30] R. Seydel, Practical bifurcation and stability analysis, vol. 5. Springer Science & Business Media, 2009.
- [31] T. Kato, *Perturbation theory for linear operators*, vol. 132. Springer Science & Business Media, 2013.
- [32] P.-Å. Wedin, "Perturbation bounds in connection with singular value decomposition," BIT Numerical Mathematics, vol. 12, pp. 99–111, 1972.
- [33] D. G. Schaeffer and I. Stewart, Singularities and groups in bifurcation theory. Springer, 1985.
- [34] J. Guckenheimer and P. Holmes, Nonlinear oscillations, dynamical systems, and bifurcations of vector fields, vol. 42. Springer Science & Business Media. 2013.
- [35] T. G. Kolda and B. W. Bader, "Tensor decompositions and applications," SIAM review, vol. 51, no. 3, pp. 455–500, 2009.
- [36] P. Kunkel, Differential-algebraic equations: analysis and numerical solution, vol. 2. European Mathematical Society, 2006.